Electronic transport in molecular systems with para- and ferromagnetic leads

2004 J. Phys.: Condens. Matter 16 4001

(http://iopscience.iop.org/0953-8984/16/23/017)

INSTITUTE OF PHYSICS PUBLISHING JOURNAL OF PHYSICS: CONDENSED MATTER

J. Phys.: Condens. Matter **16** (2004) 4001–4012 PII: S0953-8984(04)71525-8

Electronic transport in molecular systems with para- and ferromagnetic leads

W I Babiaczyk and B R Bułka

Institute of Molecular Physics, Polish Academy of Sciences, ulica M Smoluchowskiego 17, 60-179 Poznań, Poland

E-mail: iwo@ifmpan.poznan.pl (W I Babiaczyk)

Received 7 November 2003
Published 28 May 2004
Online at stacks.iop.org/JPhysCM/16/4001
DOI: 10.1088/0953-8984/16/23/017

Abstract

Using a non-equilibrium Green functions technique and the Hartree–Fock approximation, electronic transport calculations were performed for nano-devices consisting of bi-partite type molecules connected to para- and ferromagnetic leads. For the proper description of the system, the voltage drop effect on the molecule was included. A negative differential resistance in the current–voltage characteristics was found. For the system with ferromagnetic leads, bistable behaviour and significant magnetoresistance were shown.

1. Introduction

Experimental studies of the electronic transport through single molecules have attracted much interest through the last decade [1]. The main stream of research was focused on the current–voltage (I–V) characteristics of single molecules connected to metallic leads [2]. A very strong negative differential resistance (NDR) effect was observed by Chen and Reed [3] in current measurements made on triphenyl molecules connected to gold leads in the system of a break junction. The fast development of spintronics based on bulk materials and thin films indicates the direction of the near-future design of molecular devices. There is still a lack of measurements on magnetic systems based on single molecules.

Theoretical calculations of the transport phenomena in the coherent regime in single-molecule devices have focused mainly on paramagnetic systems. Transport through small molecular junctions was calculated using *ab initio* methods [4–6]. The coefficient simulating the voltage drop on the molecule, introduced by the theoreticians led by Datta, improved the results of the calculations [7]. There have been only a few works devoted to transport in systems of single molecules connected to ferromagnetic leads. However, the considered cases were either in the equilibrium state [8], or without a voltage drop on the molecule in the presence of the applied bias voltage [6].

In our work, we would like to focus on nonequilibrium spin dependent transport phenomena in devices based on a simple, bi-partite molecule attached to para- and ferromagnetic leads. The simplest molecule in this case is the two-atom molecule, where each atom is represented by a single energy level. Such a model can give information about electronic and spin polarization effects in the system, which are not obtained in the one-atom case, widely explored theoretically. We believe that, despite limitations, the two-atom model can be a useful tool in understanding transport through real systems with bi-partite molecules, like biphenyl- or other similar aromatic-type molecules, or the divanadium molecule.

The aim of our work is to provide a description of transport in magnetic systems, which can contribute to the development of spintronic nanodevices. Correlations of the spin-up and spin-down electron channels in the presence of the Coulomb repulsion on the molecule will be considered. The magnetoresistance in the ferromagnetic systems and the relations of the transport characteristics to the spin accumulation are of our particular interest, because of their applicability to electronic devices. To give a proper description of the model, we apply a voltage drop parameter in the calculations to include the screening of the electric field on the molecule, which is crucial in the formation of the NDR effect in such systems.

To obtain the current and conductance characteristics, as well as the polarization and the spin accumulation in the system, we use an analytical formula derived from the tight-binding Hamiltonian in the frame of a non-equilibrium Green functions technique. All calculations are done in the self-consistent Hartree–Fock approximation.

The paper is organized as follows. In section 2, we present the model which includes a voltage drop on the molecule, and we give a brief description of the Green functions technique. In section 3, the current and conductance characteristics, the charge accumulation and the polarization in the fully and partially screened paramagnetic systems are compared. These results are the reference data for the magnetic system considered in section 4. The current–voltage characteristics together with the magnetoresistance and the spin accumulation influence on transport for the ferromagnetic systems in the various configurations of the spin polarization alignment in the leads are presented. In section 5 we summarize the work.

2. Theoretical model

Let us briefly discuss the applicability of the two-atom model, before we describe it in detail. A bi-partite molecule is a molecule consisting of two conductive centres separated by a potential barrier from each other. Examples of such molecules can be the pure or modified biphenyl molecules, where the conductive centres are phenyl rings and the potential barrier can be the σ bond, or the –N–, –O–, –C≡C– bridge between the rings. The transport in such molecules is mainly through the highest occupied (HOMO) and lowest unoccupied (LUMO) molecular orbitals. The Fermi level of the leads lies in the HOMO–LUMO gap of the molecule. The potential drop on the phenyl ring in the presence of the applied bias voltage is much smaller than the potential drop on the barrier. Therefore this situation can be described by the two-atom model. Here, the atoms correspond to the conductive centres, and the hopping integral value between the atoms can be modified like the bond between the centres. Diagonalization of the molecular part of the Hamiltonian leads to two molecular levels, which correspond to the HOMO and LUMO in real systems. The potential drop on the two-atom molecule can be included by the application of a voltage dependent factor in the atomic energies. The applicability of the model in our calculations is, however, limited because of the usage of the Hartree–Fock approximation, which is valid only in the weak interaction regime.

Figure 1 shows schematically the system of a two-atom molecule connected to para- and ferromagnetic leads, Au and Co, respectively. The leads in the ferromagnetic system are

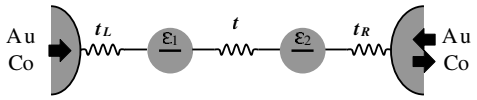

Figure 1. Model of the two-atom molecule connected to metallic leads, where in the ferromagnetic case it is possible to change the spin polarization orientation in one of them.

spin polarized and one can change the polarization alignment in the system by changing the polarization orientation in one of the leads. For simplicity each atom is represented by a single level, and such a system can be described by the Hamiltonian

$$H = \sum_{i,j}\sum_{\sigma}(t + \epsilon_i\delta_{i,j})c^{\dagger}_{i,\sigma}c_{j,\sigma} + U\sum_{i} n_{i\uparrow}n_{i\downarrow} + \sum_{k,\sigma,\alpha\in \mathrm{L,R}} \epsilon_{k\alpha}c^{\dagger}_{k\alpha,\sigma}c_{k\alpha,\sigma} + \sum_{k,\sigma}(t_{\mathrm{L}1}c^{\dagger}_{k\mathrm{L}\sigma}c_{1\sigma} + t_{\mathrm{R}2}c^{\dagger}_{k\mathrm{R}\sigma}c_{2\sigma} + \mathrm{H.c.}). \tag{1}$$

The first two terms correspond to the two-atom molecule, where the first expression describes hopping of electrons between the atoms and the potential energy of electrons, and the second one includes the on-site Coulomb interactions of the two electrons with opposite spin orientation, U being the Coulomb integral. The local atomic levels are given by $\epsilon_{i\sigma} = \epsilon^0_i - (-1)^i\eta eV/2$, where ϵ^0_i corresponds to the MO energy in the equilibrium ($V = 0$), and the coefficient $0 \leqslant \eta \leqslant 1$ describes the screening of the electrostatic potential at the molecule. $\eta = 0$ corresponds to the total screening of the molecule and $\eta = 1$ to the absence of electrostatic screening. t is the interatomic hopping parameter. The third term of (1) corresponds to electrons in the left ($\alpha = \mathrm{L}$) and right ($\alpha = \mathrm{R}$) lead. In the presence of the applied bias voltage, the chemical potentials in the leads are shifted to $\mu_{\mathrm{L}} = \mu^{(0)} + eV/2$ and $\mu_{\mathrm{R}} = \mu^{(0)} - eV/2$, where $\mu^{(0)}$ is the equilibrium value of the chemical potential. The fourth term describes the coupling of the molecule to the leads, where $t_{\mathrm{L}1}$ and $t_{\mathrm{R}2}$ correspond to the hopping integrals between the leads and the molecule. The hopping and Coulomb integrals t, t_α, U are treated as parameters which can be modified, in the frames of the applied approximations. We fix $t = 1$ eV and other parameters t_α, U are defined in relation to t.

The potential drop on the short gold atoms chain and phenyl ring between golden leads exhibits partial screening [9]. Generally, the electrostatic potential across such a nanodevice can be determined by solving the Poisson equation with the boundary conditions given by the potential difference between the metallic contacts [10]. The total potential can be divided into an applied and a self-consistent part. The applied potential part solves the Laplace equation with the known potential difference between the leads. If we assume the contacts to be semi-infinite classical metals separated by a distance (d) (capacitor), we obtain simple solutions for the applied potential $U = \frac{V}{d}x$, where x is the position relative to the midpoint between contacts. One then calculates the self-consistent part. The voltage drop factors η obtained in such a way are typically in the range 0.15–0.5. In our calculations we take $\eta = 1/3$ for the case of partial screening.

In our studies the Hartree–Fock approximation (HFA) is used. In this approximation, the calculations of the electron number on the molecule become self-consistent. The HFA leads to a simplification of the molecular term of the Hamiltonian (1) to the form

$$H^{\mathrm{HF}}_m = \sum_{i,j}\sum_{\sigma}(\tilde{\epsilon}_{i,\sigma}\delta_{i,j} + t)c^{\dagger}_{i,\sigma}c_{j,\sigma}, \tag{2}$$

with the local site energy

$$\tilde{\epsilon}_{i,\sigma} = \epsilon_i + U\langle n_{i,\overline{\sigma}}\rangle. \tag{3}$$

As one can see, the effective Hamiltonian (2) is the one-electron Hamiltonian in a self-consistent molecular field. The thermal averages $\langle n_{i,\sigma}\rangle$ are determined for the nonequilibrium case using the Keldysh Green function (see also [11]):

$$\langle n_{i,\sigma}\rangle = \int \frac{\mathrm{d}\omega}{2\pi \mathrm{i}} G^{<}_{i\sigma,i\sigma}(\omega) \qquad i = 1, 2. \tag{4}$$

The lesser Green function can be obtained from the Dyson equation and can be expressed in the general form as

$$G^{<}_{i\sigma,j\sigma} = \sum_{i',j'} G^{\mathrm{r}}_{i\sigma,i'\sigma}\Sigma^{<}_{i'\sigma,j'\sigma}G^{\mathrm{a}}_{j\sigma,j'\sigma}. \tag{5}$$

Superscripts r and a denote the retarded and advanced Green functions, respectively, and

$$G^{\mathrm{r}}(\omega) = (\mathbf{1}\omega - H^{\mathrm{HF}} - \Sigma^{\mathrm{r}})^{-1},$$

satisfying $G^{\mathrm{a}} = (G^{\mathrm{r}})^{*}$. $\mathbf{1}$ denotes the unit matrix. The lesser self-energy can be written as

$$\Sigma^{<}_{i\sigma,j\sigma}(\omega) = \mathrm{i}\delta_{i,j}[\delta_{i,1}\Gamma_{\mathrm{L}\sigma}(\omega)f_{\mathrm{L}}(\omega) + \delta_{i,2}\Gamma_{\mathrm{R}\sigma}(\omega)f_{\mathrm{R}}(\omega)], \tag{6}$$

where f_{L} and f_{R} are the Fermi distribution functions in the leads.

$$\Gamma_{\mathrm{L},\sigma}(\omega) = 2\pi t^2_{\mathrm{L},1}\rho_{\mathrm{L},\sigma}, \qquad \text{and} \qquad \Gamma_{\mathrm{R},\sigma}(\omega) = 2\pi t^2_{\mathrm{R},2}\rho_{\mathrm{R},\sigma}, \tag{7}$$

and $\rho_{\mathrm{L},\sigma}$ and $\rho_{\mathrm{R},\sigma}$ are densities of states for the electrons with given spin in the left and right lead, respectively. Using (6) we can rewrite (4) as

$$\langle n_{i,\sigma}\rangle = \langle n_{i\mathrm{L},\sigma}\rangle + \langle n_{i\mathrm{R},\sigma}\rangle.$$

The retarded (and advanced) self-energies are given by

$$\Sigma^{\mathrm{r}}_{i\sigma,j\sigma}(\omega) = \tfrac{1}{2}\mathrm{i}\delta_{i,j}\{\delta_{i,1}[\Lambda_{\mathrm{L}}(\omega) - \mathrm{i}\Gamma_{\mathrm{L}}(\omega)] + \delta_{i,2}[\Lambda_{\mathrm{R}}(\omega) - \mathrm{i}\Gamma_{\mathrm{R}}(\omega)]\},$$

where $\Lambda_{\alpha}(\omega) = \frac{1}{\pi}P\int_{-\infty}^{\dagger\infty}\mathrm{d}z\,\frac{\Gamma_{\alpha}(z)}{\omega - z}$, and $\Sigma^{\mathrm{a}} = (\Sigma^{\mathrm{r}})^{*}$. Λ_{α} is ignored in further calculations, as it only is responsible for the energy levels shift.

In order to determine the current I we apply non-equilibrium Green functions techniques. The current from the left (or equally right) lead can be determined from the time evolution of the occupation number $N_{\mathrm{L}} = \sum_{k,\sigma} c^{\dagger}_{k\mathrm{L},\sigma}c_{k\mathrm{L},\sigma}$ for electrons in the lead and can be expressed by the lesser Green function $G^{<}$. After applying the Dyson equation we can express the current as

$$I = \frac{2e}{\pi\hbar}\sum_{\sigma}\int \mathrm{d}\omega\,[f_{\mathrm{R}}(\omega) - f_{\mathrm{L}}(\omega)]\Gamma_{\mathrm{L}\sigma}(\omega)\Gamma_{\mathrm{R}\sigma}(\omega)|G^{\mathrm{r}}_{1\sigma,2\sigma}(\omega)|^2. \tag{8}$$

The conductance is determined from $\mathcal{G} = \partial I/\partial V|_{V=0}$.

In our calculations we focus on the influence of magnetic polarization in the leads on the transport characteristics. For the sake of simplicity and clearness of the work the electron–phonon coupling is neglected in our model. Calculations are addressed to the low temperature limit, where the vibrational mode contribution to the non-equilibrium current is dominated by the polarization effects. However, the formalism of the Green functions used in this work can also be applied to the case where electron–phonon coupling is included. Such studies were performed on the non-magnetic single-level model and can be found in [12].

3. Transport in a system with paramagnetic leads

In systems with real molecules, the transport is mainly through the MOs close to the Fermi level in the leads. In our calculations, the system is described by a two-atom model, where each atom is represented by a single energy level. We impose high overlapping (large hopping

integral value $t = 1$ eV) of ϵ_1 and ϵ_2, which causes hybridization into bonding $\tilde{\epsilon}_-$ (BLs) and antibonding $\tilde{\epsilon}_+$ (ABLs) levels, where $\tilde{\epsilon}_\pm = [\tilde{\epsilon}_1 + \tilde{\epsilon}_2 \pm \sqrt{(\tilde{\epsilon}_1 - \tilde{\epsilon}_2)^2 + 4t^2}]/2$. The BL and ABL in our case correspond to the HOMO and LUMO in the real molecular system. We assume the Fermi level of the leads to be inside the $\Delta\epsilon = \tilde{\epsilon}_+ - \tilde{\epsilon}_-$ gap, closer to the ABL as occurs in real systems. Because of the coupling to the contacts, the BL and ABL are represented with the Lorentzian density of states, i.e. the imaginary part of the appropriate Green function.

The Coulomb repulsion leads to a pinning of the local site self-consistent energy levels to the chemical potentials of the source and drain leads. The pinning extends over finite voltage regions of the range of U/e. This continuous shift of the levels is caused by the $U\langle n_{i,\overline{\sigma}}\rangle$ term in the local site energy. For stronger Coulomb interactions ($U \geqslant t$) one can expect a more complex electronic structure, in which many-electron states occur, separated from the one-electron states by energy of the order of U. Many-body effects and electronic correlations are omitted in the Hartree–Fock approximation. The present studies are, therefore, confined to weak interactions, where the HFA gives reliable results and the single-electron picture is still valid. The choice of the particular value of Coulomb integral for the model is somewhat arbitrary, i.e. $0 < U < t$. In our numerical calculations, we assume $U = 0.2$ eV, which ensures that the system is in the low interaction limit, and, on the other hand, all features connected with the Coulomb repulsion can be observed. A detailed discussion of the effects of Coulomb repulsion in multiatomic molecules for a wide range of U values is given in [11].

In figure 2(a) we show the current and the conductance characteristics for a system with screening of the electric field, which corresponds to $\eta = 0$. In the low voltage range (LVR) the chemical potentials of the leads are in the energy gap (BL $< \mu_R < \mu_L <$ ABL) and the current is infinitesimally small. For higher voltages the chemical potential of the left lead μ_L reaches the ABL and one can observe a step in the I–V curve and the corresponding peak in the $\mathcal{G}$–V plot. In this voltage range the self-consistent level ABL is pinned to μ_L and its position is shifted with the voltage (ABL $\approx \mu_L$ and BL $< \mu_R$). This voltage region is called (after [11]) the incomplete one-channel transport range (I1CTR) because electrons fill the ABL partially and only a part of the electronic spectrum participates in transport. When the voltage further increases the system goes to the complete one-channel transport range (1CTR) with a plateau seen in the I–V curve. In this voltage region the whole spectrum of the ABL participates in transport and the molecule has two electrons on average. Another step in the I–V curve, and a peak in the $\mathcal{G}$–V curve, occurs when the chemical potential in the right lead μ_R reaches the BL (BL $\approx \mu_R <$ ABL $\leqslant \mu_L$). Because the transport is through the whole spectrum of the ABL and only partially through the BL, this region is called the incomplete two-channel transport range (I2CTR). The complete two-channel transport region (2CTR) can be observed for very high voltages, when both states are deep inside the bias voltage window, $\mu_R \ll$ BL $<$ ABL $\ll \mu_L$ and the current saturates.

If the system is partially screened, which corresponds to $\eta = 1/3$, the characteristics are modified as shown in figure 2(b). The current exhibits a negative differential resistance effect, seen after the second step in the I–V characteristics. The NDR effect is the consequence of the broadening of the $\Delta\epsilon$ energy gap due to the shift of local energy levels. This also results in the shift of the current steps and conductance peaks.

In figures 3(a) and (b) the average number of electrons and the electronic polarization are shown. In the LVR the total number of electrons $n_t = n_1 + n_2$ is equal to two and the molecule is chemically neutral. Despite the infinitesimally small current (i.e. transmission close to zero), an electric field is present in the system due to the applied bias voltage. This results in a spatial charge shift towards the drain lead, and the polarization $p = n_1 - n_2$ is negative. For higher voltages, the ABL pins to the chemical potential in the source lead which corresponds to the I1CTR, and n_t and p increase. With the increase of the voltage the

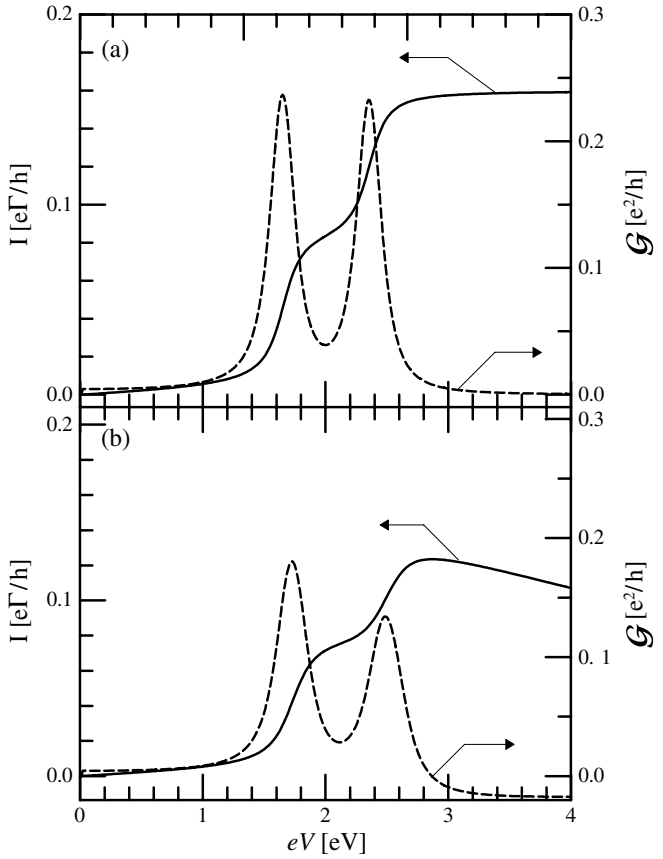

Figure 2. Current–voltage (solid curves) and conductance–voltage (dashed curves) characteristics of the paramagnetic system for cases of $\eta = 0$ (a) and $\eta = 1/3$ (b). The transfer rates between the sites and the leads in (a) and (b) are taken as $\Gamma_L = \Gamma_R = 0.04$ eV, and the site energies $\epsilon_1 = \epsilon_2 = -0.3$ eV. We assume $t = 1$ eV and the Coulomb repulsion parameter $U = 0.2$ eV.

ABL depins from the chemical potential and the system enters the 1CTR. In this region the number of electrons and the polarization remain almost constant (a detailed discussion of the conditions of the pinning of the molecular levels to the chemical potentials in the leads is given in [11]). When the chemical potential of the drain lead reaches the BL, analogous processes take place. The BL pins to the chemical potential and the system enters the I2CTR, and the 2CTR when it depins for higher voltage. The average number of electrons n_t gradually returns to two, and the polarization p gradually increases, changing sign for very high voltages. When the electrostatic potential is screened, changes of the polarization only result from electron transport. Thus, the polarization for $\eta = 0$ takes very small values. For the $\eta = 1/3$ case, the electrostatic potential magnifies the spatial charge displacement. The abrupt increase of the polarization for higher voltages in that case also results from the energy gap $\Delta\epsilon$ widening with the voltage. The electron hopping between the atoms is quenched, which causes a charge accumulation on the atom closer to the source lead.

Let us consider the situation when the Fermi level is above the ABL. The total electron number n_t is equal to four at equilibrium. At the points where the chemical potential reaches the ABL and BL energies n_t drops to three, and stabilizes at the value of two for higher

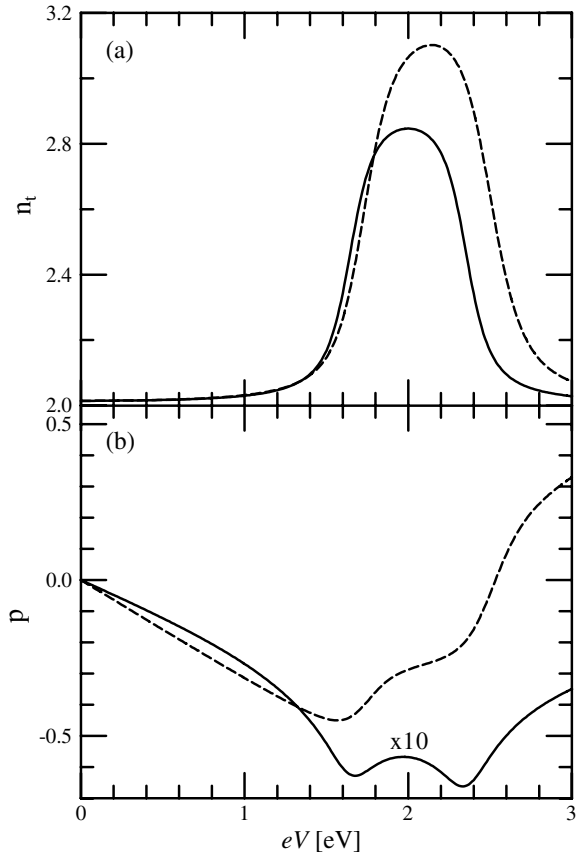

Figure 3. Total number of electrons (a) and electronic polarization (b) of the paramagnetic system for $\eta = 0$ (solid) and $\eta = 1/3$ (dashed curves). The values of the polarization in the $\eta = 0$ case are multiplied by 10 to show the characteristic features. All parameters are the same as for figure 2.

voltages. The polarization is positive for low voltages, because the transport through the atom closer to the drain lead is completely blocked. When the voltage is increased, the drain lead's chemical potential reaches the ABL, and when the system enters the 1CTR the polarization drops and changes sign. Transport through the atom closer to the drain lead is still blocked. After reaching the BL, the system is in the 2CTR and the polarization increases again, being positive for high voltages. The current– and the conductance–voltage characteristics do not change much. The steps in the current, as well as the peaks in the conductance, experience a shift due to the shift of the ABL and BL positions.

The situation when the Fermi level of the leads at equilibrium is closer to the BL or below the energy gap can be described in a similar way as former cases using electron–hole symmetry. For example, the number of electrons drops to one in the one-channel transport range, the polarization is opposite, and the current and conductance do not change in a qualitative way.

4. Spin-dependent transport

Spin-dependent transport widens the spectrum of possible applications of molecular nanodevices in electronics. The external magnetic field or the magnetic atoms on the molecule

split the molecular levels. The case of a single quantum dot device in the presence of a magnetic field was discussed in detail in [13]. One can expect a similar situation for transport through a single-atomic system. Spin-dependent transport can also be introduced by replacing the non-magnetic leads with the magnetic ones. In our work we use ferromagnetic leads and a non-magnetic bi-partite molecule. The imbalance of the spin populations in the leads together with the Coulomb repulsion on the atomic sites remove the spin degeneration of the BL and ABL. In this section, we will denote the levels as BL$\uparrow$ and BL$\downarrow$ (ABL$\uparrow$ and ABL$\downarrow$) with respect to the up- and down-spin orientations of the incident electrons.

Because BL$\uparrow$ and BL$\downarrow$, as well as ABL$\uparrow$ and ABL$\downarrow$, are very close to each other, one can only distinguish between the two- and four-channel transport regions. The incomplete two-channel transport region (I2CTR) corresponds to the situation where the transport is through the major part of the ABL$\downarrow$ spectrum and a smaller part of the ABL$\uparrow$ (ABL$\downarrow \approx \mu_{\mathrm{L}} <$ ABL$\uparrow$ and BL$\uparrow\downarrow < \mu_{\mathrm{R}}$). In the ferromagnetic case, both ABLs are pinned in the vicinity of the chemical potential μ_{L} in the region of the voltage range of the order U. The ABLs' and chemical potential's μ_{L} relative positions are determined by the self-consistent procedure. The system enters the complete two-channel transport region (2CTR) when both ABL$\downarrow$ and ABL$\uparrow$ depin from μ_{L} and fully participate in the transport. For higher voltages one can observe an analogous situation for the BLs. BL$\uparrow$ and BL$\downarrow$ pin in the vicinity of the chemical potential μ_{R} in the right lead, the transport is through the major part of the BL$\uparrow$ spectrum and a smaller part of BL$\downarrow$. The system is in the incomplete four-channel transport region (I4CTR). For very high voltages, the system reaches the complete four-channel transport region (4CTR), where $\mu_{\mathrm{R}} \ll$ BL$\uparrow\downarrow <$ ABL$\uparrow\downarrow \ll \mu_{\mathrm{L}}$.

The current–voltage characteristics for the parallel (P) and the antiparallel (AP) spin polarization alignment in the leads are shown in the figures 4(a) and (b). The leads in our case are cobalt. The densities of states (DOS) for ferromagnetic Co, needed for calculating transfer efficiencies (7), are approximated by the constant values: $\rho_{\uparrow} = 0.174$ states eV^{-1} for up-spin electrons and $\rho_{\downarrow} = 0.735$ states eV^{-1} for down-spin electrons. DOS were determined from band structure calculations performed using the tight binding version of the linear muffin-tin orbital method in the atomic sphere approximation [14].

The current in the P configuration (figure 4(a)) is infinitesimally small in the LVR, and increases when the chemical potential in the source lead reaches the ABL. When the voltage is increased, the current enters a region of bistable behaviour and a hysteresis can be observed. Further increase of the voltage leads to another step without hysteresis. After a small plateau, hysteresis occurs once again in the third step, where the current shows bistable behaviour, and is absent in the fourth step. The bistable solutions can only appear in the I2CTR and I4CTR, for large Coulomb interactions [15]. In the enlarged inset of the current plot (figure 4(a)) the three solutions obtained in the I4CTR can be seen. When one increases the voltage, the solution corresponding to higher current is engaged in the transport. If the voltage decreases, the solution corresponding to smaller current takes part in the transport. Following the arrows in the inset of figure 4(a), which indicate the voltage direction, the hysteresis loop can be formed. For very high voltages, in the complete four-channel transport range, one can observe the NDR effect due to the widening of the energy gap.

The current in the AP configuration, shown in the figure 4(b), increases abruptly when the chemical potential in the source lead reaches the ABL. In this case, however, it does not exhibit a hysteresis, but an extra step appears in the characteristic due to the spin accumulation. With the voltage increase, one can observe a plateau in the 2CTR and another two steps, when the chemical potential in the drain lead reaches the BL. In both cases, the first of the steps is due to the spin accumulation effect on the current, and the other one is due to the entering of the two- or four-channel transport range. For higher voltages, the current also exhibits an NDR effect.

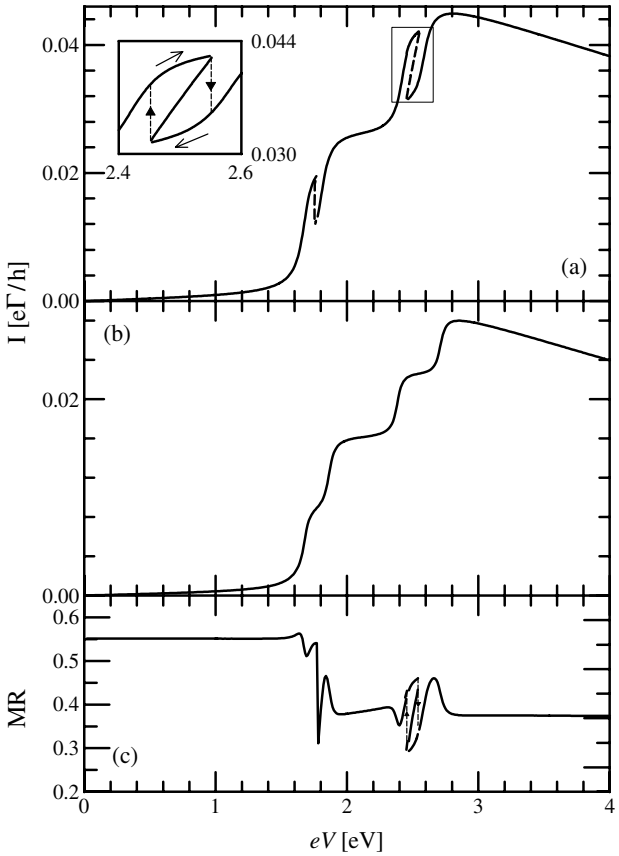

Figure 4. Current–voltage characteristics of the ferromagnetic system for the parallel (a) and antiparallel (b) spin polarization alignment in the Co leads. The transfer rates between the sites and the leads are taken as $\Gamma_{\alpha\uparrow} = 0.005$ eV and $\Gamma_{\alpha\downarrow} = 0.023$ eV, and the site energies $\epsilon_1 = \epsilon_2 = -0.3$ eV. The current is normalized with $\Gamma = \sum_{\alpha,\sigma} \Gamma_{\alpha,\sigma}$. We assume $t = 1$ eV and the Coulomb repulsion parameter $U = 0.2$ eV. Below, the magnetoresistance (c) in the system.

The magnetoresistance (MR), defined as the relative difference of the current in the P and AP configuration of the polarization alignment in the leads, $\mathrm{MR} = (I_\mathrm{P} - I_\mathrm{AP})/I_\mathrm{AP}$, is shown in figure 4(c). In the LVR the MR is large. When the system enters the I2CTR, the MR reflects the first step-like structure in the AP current and a small peak can be observed. The following large dip is the result of the current drop in the bistable range. Hysteresis occurs in this region; however, it is very narrow. In the 2CTR, the MR stabilizes. The situation is repeated in the I4CTR; hysteresis is now well seen. The magnitude of the MR in the 2CTR and 4CTR is constant, because the rate of electrons with certain spin orientation transferred from the source to the drain lead for P and AP polarization alignment remains the same.

As the DOS for the spin-up and -down electrons can be different in both leads, spin accumulation (SA) is formed by electrons of spin σ which could not diffuse to the drain lead because of the smaller transfer efficiency ($\Gamma_{\mathrm{L},\sigma} > \Gamma_{\mathrm{R},\sigma}$). The SA is defined as $s = \sum_i (\langle n_{i,\downarrow}\rangle - \langle n_{i,\uparrow}\rangle)$ (the majority spin in our case is $\downarrow$). As the average occupation of the site depends on the contacts' efficiencies, one can observe SA when $\Gamma_{\alpha,\sigma} \neq \Gamma_{\alpha,-\sigma}$, i.e. in the case of the ferromagnetic leads. Spin-flip processes can reduce the SA, but they are not taken into account in our studies.

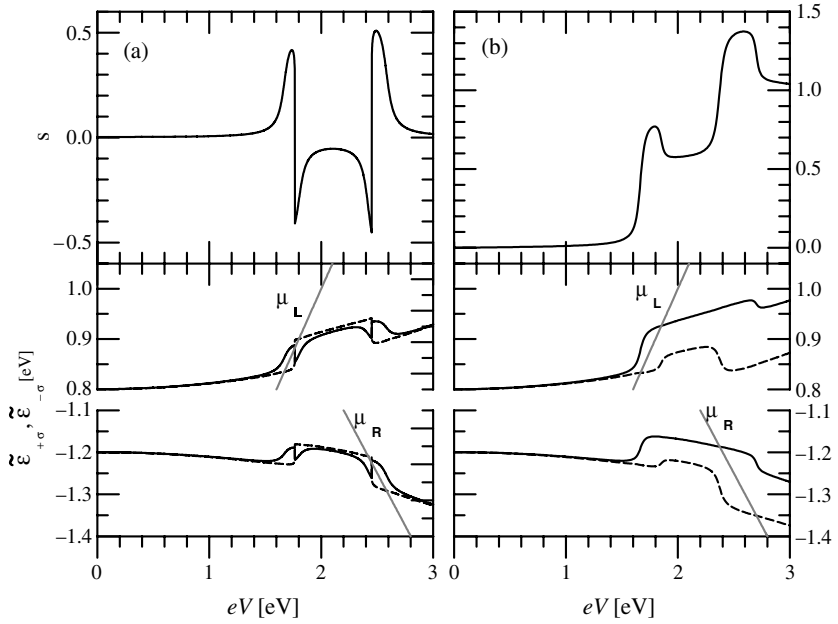

Figure 5. Spin accumulation (upper plots) of the ferromagnetic system in the P (a) and AP (b) alignment of the polarization in the leads together with $\tilde{\epsilon}_{\pm,\sigma}$ energy plots (lower plots), where $\mu_{\mathrm{L}} = E_{\mathrm{F}} + V/2$ and $\mu_{\mathrm{R}} = E_{\mathrm{F}} - V/2$ denote the position of the chemical potentials in the left and right lead, respectively (grey lines). Solid curves correspond to $\tilde{\epsilon}_{\pm,\uparrow}$ and dashed to $\tilde{\epsilon}_{\pm,\downarrow}$. The transfer parameters are the same as in figure 4.

The SA in the system is shown in figures 5(a) and (b), together with the BL and ABL energies. The influence of the SA on the I–V characteristics can be observed by comparing the current plot in figure 2(b) with figures 4(a) and (b). The occurrence of SA in the system enriches the I–V curve with extra NDR peaks and extra steps in the P and AP configuration, respectively. In the P configuration (see figure 5(a)), the SA is close to zero in the LVR. With the voltage increase the chemical potential in the source lead μ_{L} approaches the ABL. μ_{L} reaches the ABL$\downarrow$ and the SA increases. In the I2CTR the SA drops rapidly and changes sign. Because the coupling $\Gamma_{\mathrm{L}\downarrow} \gg \Gamma_{\mathrm{L}\uparrow}$, the ABL$\downarrow$ local density of states forms a wide and flat band, while the ABL$\uparrow$ a narrow and high one. Hence, when the chemical potential in the source lead reaches the ABL$\uparrow$, the number of spin-up electrons increases rapidly and exceeds the spin-down number. Due to the Coulomb repulsion on the sites, the position of the levels, for such an occupation ratio, is reversed. BL$\downarrow$ and BL$\uparrow$ reflect the change as well. With the voltage increase the system enters the 2CTR, and the SA increases due to the diminishing difference in the transferred spin-up and spin-down electron ratio. The positions of the levels remain reversed until the chemical potential in the drain lead reaches the BL. The behaviour of the SA in the I4CTR reflects the MO levels and the chemical potential in the leads' relative configuration and is thus contrary to the I2CTR case. The SA drops almost to zero when the transport enters the 4CTR, remaining zero for high voltages.

In the AP configuration of the spin polarization in the leads, the SA is close to zero in the LVR (see figure 5(b)). On increasing the voltage, the number of the majority spin electrons increases, and so does the SA. When the chemical potential in the source lead reaches the ABL (I2CTR), both the ABL$\uparrow$ and the ABL$\downarrow$ are shifted up and the SA increases faster. Unlike in the P configuration, the levels do not switch. The number of spin-up electrons cannot exceed

the number of spin-down electrons. In the 2CTR, the SA drops. When the chemical potential in the drain lead reaches the BL and the system enters the I4CTR, another step in the SA plot appears.

The obtained SA characteristic is different from the case of a single atomic molecule (or single quantum dot), where the SA is zero for any voltage in the AP configuration. The difference results from different broadening of the local atomic levels for both cases. In the two-atomic system, the broadening of the level in the left atom depends mainly on the coupling $\Gamma_{L,\sigma}$ with the left lead, whereas for the right atom it depends on $\Gamma_{R,\sigma}$. As the couplings for the left and right atom are different in the AP case ($\Gamma_{L,\sigma} > \Gamma_{R,\sigma}$, where σ denotes the majority spin sign), the SA is always positive for positive voltage, or negative for negative voltage.

The mechanisms of forming the SA described above are valid for the unscreened electrostatic potential case as well as for the screened case. For the screened case, however, the SA in the AP configuration remains constant for very high voltages, because the number of spin-up and spin-down electrons stabilizes at the same value, due to the constant BL–ABL gap.

5. Summary

Nonequilibrium spin-dependent transport calculations in devices based on bi-partite type molecules attached to para- and ferromagnetic leads were performed. The bi-partite molecule was described by the two-atom molecule model. For all considered cases the NDR effect was obtained, which is connected with the application of a voltage drop inside the molecule. It was shown that in the case of parallel alignment of the spin polarization in the leads, the current can exhibit bistable behaviour connected with the pinning of the atomic levels to the Fermi energy. Such features are caused by Coulomb repulsion on the atoms in the incomplete two- and four channel transport regimes (I2CTR and I4CTR). We predict that sweeping the current in a positive and then negative direction gives rise to the hysteresis loops in these regimes. The current in the antiparallel configuration does not exhibit bistable behaviour. The bistable regions give the opportunity to switch the current between two values in a narrow voltage range, and the system can therefore be interesting as a practical switch or as a spin filter, in the P configuration. It was also shown that the current in the P configuration is higher than in the AP case, leading to a positive magnetoresistance in the system. Interesting results are the SA characteristics obtained for the two-atom molecule. The character of the SA is different than in the one-atom case, due to the different mechanism of the coupling of atomic levels to the leads. Because of the potential barrier between the atoms, the broad levels do not overlap and the effects of the separation can be observed in the SA. In the P case, the SA is close to zero in the LVR and 2CTR and 4CTR, changing sign with filling up the successive levels, but it exhibits rapid changes in the I2CTR and I4CTR. In the AP case the SA is always positive (for positive voltage), increasing on entering the successive transport channels.

Acknowledgments

The authors would like to thank A Szajek for providing the calculations of the densities of states for the ferromagnetic materials, and S Lipiński and P Stefański for helpful discussions. The work was partially supported by the Committee for Scientific Research under Grant No. 2 P03B 118 25 (WIB) and PBZ KBN 044 P03 2001 (BRB).

References

[1] Joachim C, Gimzewski J K and Aviram A 2000 *Nature* **408** 541
[2] Datta S, Tian W, Hong S, Reifenberger R, Henderson J I and Kubiak C P 1997 *Phys. Rev. Lett.* **79** 2530

Kergueris C, Bourgoin J-P, Palacin S, Esteve D, Urbina C, Magoga M and Joachim C 1999 *Phys. Rev.* B **59** 12505
Reichert J, Ochs R, Beckmann D, Weber H B, Mayor M and von Löhneysen H 2002 *Phys. Rev. Lett.* **88** 176804
[3] Chen J, Reed M A, Rawlett A M and Tour J M 1999 *Science* **286** 1550
Reed M A, Chen J, Rawlett A M, Price D W and Tour J M 2001 *Appl. Phys. Lett.* **78** 3735
[4] Derosa P A and Seminario J M 2001 *J. Phys. Chem.* B **105** 471
Larade B, Taylor J, Merez H and Guo H 2001 *Phys. Rev.* B **64** 075420
[5] Lang N D and Avouris Ph 2000 *Phys. Rev. Lett.* **84** 358
Di Ventra M, Pantelides S T and Lang N D 2000 *Phys. Rev. Lett.* **84** 979
Di Ventra M, Kim S-G, Pantelides S T and Lang N D 2001 *Phys. Rev. Lett.* **86** 288
Heurich J, Cuevas J C, Wenzel W and Schön G 2002 *Phys. Rev. Lett.* **88** 256803
[6] Pati R, Senapati L, Ajayan P M and Nayak S K 2003 *Phys. Rev.* B **68** 100407(R)
[7] Tian W, Datta S, Hong S, Reifenberger R, Henderson J I and Kubiak C P 1998 *J. Chem. Phys.* **109** 2874
Xue Y, Datta S, Hong S, Reifenberger R, Henderson J I and Kubiak C P 1999 *Phys. Rev.* B **59** R7852
[8] Bułka B R and Lipiński S 2003 *Phys. Rev.* B **67** 024404
Babiaczyk W I and Bułka B R 2002 *Acta. Phys. Pol.* A **102** 597
Kikoin K and Avishai Y 2001 *Phys. Rev. Lett.* **86** 2090
[9] Damle P S, Ghosh A W and Datta S 2001 *Phys. Rev.* B **64** 201403
[10] Paulsson M, Zahid F and Datta S 2004 *Nanoscience, Engineering and Technology Handbook* at press
[11] Kostyrko T and Bułka B R 2003 *Phys. Rev.* B **67** 205331
[12] Zhu J-X and Balatsky A V 2003 *Phys. Rev.* B **67** 165326
[13] Świrkowicz R, Barnaś J and Wilczyński M 2003 *Phys. Status Solidi* a **196** 105
[14] Szajek A, private calculations using: Krier G, Jepsen O, Burkhardt A and Andersen O K 1995 *The TB-LMTO-ASA Program* source code version 4.7 (Max Plank-Institut für Festkörperforschung, Stuttgart, Germany)
[15] Bułka B and Kostyrko T 2003 unpublished